Dalton Transactions

PAPER

View Article Online
View Journal

Cite this: DOI: 10.1039/c8dt04807j

Synthesis of new Mn_{19} analogues and their structural, electrochemical and catalytic properties†

Elodie Chevallot-Beroux,[a] Ayuk M. Ako,[b] Wolfgang Schmitt,[b] Brendan Twamley,[b] Joseph Moran,[a] Boudon Corinne,[c] Laurent Ruhlmann[c] and Samir Mameri *[d]

Received 6th December 2018,
Accepted 13th February 2019

DOI: 10.1039/c8dt04807j

rsc.li/dalton

We report the synthesis and structural characterisation of new Mn_{19} and $Mn_{18}M$ analogues, $[Mn^{III}_{12}Mn^{II}_{7}(\mu_4\text{-}O)_8(\mu_3\text{-}OCH_3)_2(\mu_3\text{-}Br)_6(HL^{Me})_{12}(MeOH)_6]Br_2$ (**2**) and $[Mn^{III}_{12}Mn^{II}_{6}Sr(\mu_4\text{-}O_8(\mu_3\text{-}Cl)_8(HL^{Me})_{12}(MeCN)_6]Cl_2$ cluster (**3**), where H_3L^{Me} is 2,6-bis(hydroxymethyl)-*p*-cresol. The electrochemistry of **2** and **3** has been investigated and their activity as catalysts in the oxidation of benzyl alcohol has been evaluated. Selective oxidation of benzyl alcohol to benzaldehyde by O_2 was achieved using 1 mol% of catalyst with conversions of 74% (**2**) and 60% (**3**) at 140 °C using TEMPO as a co-catalyst. No partial conversion of benzaldehyde to benzoic acid was observed. The results obtained revealed that different operative parameters – such as catalyst loading, temperature, time, solvent and the presence of molecular oxygen – played an important role in the selective oxidation of benzyl alcohol.

Introduction

Manganese-based coordination clusters continue to attract intense research interest because they serve as models for various metalloenzymes,[1] and sometimes show interesting magnetic properties.[2,3] For some time now, we have developed a variety of homo- and hetero-metallic Mn clusters using phosphonate ligands,[4–8] and the H_3L^R ligand system based on 2,6-bis(hydroxymethyl)-4-R-phenol (where R is the substituent at the 4-position).[9–14] Among others, we are particularly interested in the coordination chemistry of the H_3L^R ligand system because of the variable modes (μ_2 or μ_3) of coordination provided by this oxido-rich molecule that lead to the isolation of organic–inorganic hybrid architectures with multiple metal centres. To this end, we have successfully developed reproducible routes for the syntheses of homometallic $Mn_{19}(R)$ (R = H, Me, I, F, OMe, SMe)[9–12] and/or heterobimetallic $Mn_{18}M$ (M = Cd, Sr, Dy, Lu, Y) aggregates[13,14] using this ligand system. The Mn_{19} and $Mn_{18}M$ systems represent a family of materials with attractive structural and magnetic properties which may open new gateways to coordination complexes exhibiting a broad range of physicochemical properties appropriate for developing applications in data storage,[15] catalysis,[16] piezoelectricity,[17] and superconductivity.[18] Experimental and theoretical studies have revealed that the achievement of the maximum possible ground spin state of S_T = 83/2 for the mixed-valence Mn_{19} system is insensitive to replacement of its eight μ_3-N_3 ligands of the original Mn_{19} aggregate $[Mn^{III}_{12}Mn^{II}_{7}(\mu_4\text{-}O)_8(\mu_3\text{-}N_3)_8(HL^{Me})_{12}(MeCN)_6]Cl_2$ (**1**) by μ_3-Cl, μ_3-Br, μ_3-OH or μ_3-OMe, substantiating that the ferromagnetic interactions are mediated mainly by the internal (μ_4-O) ligands. Indeed, ESI-MS studies have further demonstrated the robustness of the inorganic $\{Mn^{III}_{12}Mn^{II}_{7}(\mu_4\text{-}O)_8\}$ core in the Mn_{19} and $Mn_{18}Y$ species as these maintain their integrity even in relatively reactive solvents ($MeOH/H_2O$).[12] While structural studies on these systems have focused on the modification of peripheral organic ligands, the manipulation of the face-bridging ligands as well as the selective incorporation of heterometals in view of assessing their influence on the magnetic properties of the resulting compounds,[9–14] their potential as catalysts has not been explored, despite their structural (core robustness, labile apical ligands, ease of functionalization) and electronic (mixed-valence Mn) attributes. Manganese species have been shown to function as catalysts for organic and water oxidations in the presence of a variety of oxidants,[19] and have also been used as electrocatalysts.[20,21]

[a]*Laboratory of Chemical Catalysis, University of Strasbourg, ISIS UMR 7006, 8 allée Gaspard Monge, Strasbourg 67083, France. https://isis.unistra.fr/laboratoire-de-catalyse-chimique-joseph-moran/*

[b]*School of Chemistry & CRANN, University of Dublin, Trinity College, Dublin 2, Ireland. http://www.chemistry.tcd.ie/staff/schmittw/*

[c]*Laboratoire d'Electrochimie et de Chimie Physique du Corps Solide, Institut de Chimie, UMR CNRS 7177, Université de Strasbourg, 4 rue Blaise Pascal, CS 90032, Strasbourg 67081, France. http://institut-chimie.unistra.fr/equipes-de-recherche/lecpcs-electrochimie-et-chimie-physique-du-corps-solide/*

[d]*IUT Robert Schuman, Département Chimie, 72 route du Rhin, BP 70028, Illkirch 67411, France. E-mail: mameri@unistra.fr; Tel: +33-695-981-651*

†Electronic supplementary information (ESI) available: Experimental section, single-crystal X-ray crystallographic measurements, X-ray powder diffraction, electrochemical studies, chemical oxidation studies, infrared spectral analysis, mass spectrometry. CCDC 1882361 and 1882362. For ESI and crystallographic data in CIF or other electronic format see DOI: 10.1039/c8dt04807j

A variety of catalytic methods have been developed to harness molecular oxygen for the partial oxidation of alcohols to aldehydes, or for their complete oxidation to yield carboxylic acids.[22] Along these lines, the partial oxidation of benzyl alcohol to benzaldehyde with molecular oxygen has been particularly well-studied, due to the role of the latter as a versatile intermediate in the pharmaceutical and agrochemical industries.[23–26] A great many factors such as catalyst, temperature, solvent and oxidant play an important role in the reaction.[27–33] Homometallic Mn and heterometallic Mn/M (M = Ce) complexes and many other metal-oxo complexes have also been widely used as oxidants in chemical transformations such as the partial dehydrogenation of primary alcohols into their corresponding aldehydes.[33–37] To this end, we have chosen the partial oxidation of benzyl alcohol as a model substrate to study the catalytic activity of new analogues of the structural robust Mn_{19} and $Mn_{18}Sr$ coordination clusters, namely, $[Mn^{III}_{12}Mn^{II}_{7}(\mu_4\text{-}O_8(\mu_3\text{-}OCH_3)_2(\mu_3\text{-}Br)_6(HL^{Me})_{12}(MeOH)_6]Br_2$ (**2**) and $[Mn^{III}_{12}Mn^{II}_{6}Sr(\mu_4\text{-}O_8(\mu_3\text{-}Cl)_8(HL^{Me})_{12}(MeCN)_6]Cl_2$ (**3**). Compounds **2** and **3** are mixed-valent, comprising multiple Mn^{II}/Mn^{III} centres and thus have the ability to transfer (multiple) electrons. Moreover, the core features labile solvent molecules that may facilitate the coordination of incoming substrates. The electrochemical properties of **2** and **3** have been investigated, and their catalytic activity in the oxidation of benzyl alcohol has been evaluated, to test the potential of these compounds in molecular catalysis.

Experimental

Reagents and analytical methods

All chemicals and solvents were of reagent grade and purchased from Sigma-Aldrich and used without further purification. Infrared spectra were recorded on a PerkinElmer Spectrum One FT-IR spectrometer using either a universal ATR sampling accessory or a diffuse reflectance sampling accessory. Data were collected and processed using Spectrum v5.0.1 (2002 PerkinElmer Instrument LLC) software. The scan rate was 16 scans per minute with a resolution of 4 scans in the range 4000–500 cm^{-1} (ATR measurements were performed on an ATR IRAffinity-1 instrument (Shimadzu Scientific Instruments). The analyzed samples were prepared by deposition of powder or crystals directly onto the sample plate surface). The standard abbreviations were used to describe the intensities: s, strong; m, medium; w, weak; br, broad. Elemental analyses (CHN) were performed at the School of Chemistry and Chemical Biology, University College Dublin (Ireland), using Exeter Analytical CE 440 elemental analyser. GC-MS analysis were performed on a GC System 7820A (G4320) connected to a MSD block 5977E (G7036A), using Agilent High Resolution Gas Chromatography Column: PN 19091S – 433UI, HP – 5MS UI, 28 m × 0.250 mm, 0.25 micron, SN USD 489634H. All samples were prepared in ethyl acetate (200 μL sample volume). The analysis was carried out on a splitless 1 μL injection volume with an injection port temperature 250 °C. Column oven temperature program was as follows: 60 °C for 1 min, ramped at 30 °C min^{-1} to 310 °C with 3 min hold, with a total running time of 12.33 min. The mass spectrometer was turned on after 2 min and was operated at the electron ionization mode with quadrupole temperature of 150 °C. Data acquisition was performed in the full-scan mode (50–500). Hydrogen (99.999% purity) was used as carrier gas at a constant flow rate of 1.5 mL min^{-1}.

Synthesis of $[Mn^{III}_{12}Mn^{II}_{7}(\mu_4\text{-}O)_8(\mu_3\text{-}OCH_3)_2(\mu_3\text{-}Br)_6(HL^{Me})_{12}(MeOH)_6]Br_2$ (2)

$MnBr_2{\cdot}4H_2O$ (0.2 g, 1 mmol, 1.0 equiv.), Et_3N (0.1 g, 1 mmol, 1.0 equiv.) and 2,6-bis(hydroxymethyl)-4-methylphenol (0.17 g, 1 mmol, 1.0 equiv.) were respectively added, under stirring, to a MeCN/MeOH solution (25 mL/5 mL). The resulting slurry was stirred for 1 h at RT, before being heated at reflux for 2 h, to afford a dark brown solution, which was cooled and filtered. Dark brown crystals of **2** were obtained after 48 h slow evaporation at RT. The crystals were filtered, washed and dried. Yield: 30% (based on Mn). Elemental analysis (%) calc. for $C_{137}H_{184}Br_8Mn_{19}N_{10}O_{53}$: C 36.55; H 4.12; N 3.11; found: C 36.62; H 4.23; N 3.25. Selected IR data (KBr pellet, cm^{-1}) 600 (s), 800 (s), 1050 (m), 1100 (m), 1211 (s), 1409 (s), 1610 (m), 2800 (w), 3300 (w, br).

Synthesis of $[Mn^{III}_{12}Mn^{II}_{6}Sr(\mu_4\text{-}O_8(\mu_3\text{-}Cl)_8(HL^{Me})_{12}(MeCN)_6]Cl_2$ (3)

A slurry of $MnCl_2{\cdot}4H_2O$ (0.2 g, 1 mmol, 1.0 equiv.), Et_3N (0.1 g, 2 mmol, 2.0 equiv.), 2,6-bis(hydroxymethyl)-4-methylphenol (0.17 g, 1 mmol, 1.0 equiv.) in a solvent mixture of MeCN and MeOH (25 mL/5 mL) was stirred for 30 min at RT, and $Sr(NO_3)_2$ (0.11 g, 0.5 mmol, 0.5 equiv.) was added. The resulting mixture was further stirred for an additional 1 h, then heated at reflux for 2 h. The dark brown mixture was cooled and filtered. After a 24 h slow evaporation at RT, dark brown crystals of **3** suitable for X-ray diffraction analysis were obtained. Yield: 40% (based on Mn). Elemental analysis (%) calc. for $C_{127}H_{154}Cl_8Mn_{18}N_6O_{51}Sr$ (**3**): C 38.71; H 3.94; N 2.13; found: C 38.62; H 3.63; N 2.25. FT-IR (cm^{-1}): 610 (s), 740 (s), 990 (s), 1050 (s), 1248 (s), 1495 (s), 1600 (m), 2812 (w), 3300 (s, br).

Single-crystal X-ray crystallographic measurements

X-ray structural analyses for crystals of **2** (TCD304) and **3** (TCD 716) were performed on at 100 K on a Bruker APEX DUO CCD and Bruker D8 Quest ECO diffractometer respectively (Mo-K_α λ = 0.71073 Å). The maximum resolution for data collection was 0.77 Å with data collected using ω and φ scans for **2** and 0.80 Å using ω scans only for **3**.

The data were reduced and processed using the Bruker APEX suite of programs.[38] Multi-scan absorption corrections were applied using SADABS.[39] Using Olex2,[40] the structure was solved with the XT[41] structure solution program using Intrinsic Phasing and refined with the XL[42] refinement package using Least Squares minimisation. All non-hydrogen atoms were refined anisotropically. Hydrogen atoms were placed in calculated positions and refined with a riding

model, with isotropic displacement parameters equal to either 1.2 or 1.5 times the isotropic equivalent of their carrier atoms.

The data were solved in the monoclinic space group $P2_1/n$ (**2**) trigonal space group $R\bar{3}$ (**3**). In the structure of **2**, uncoordinated MeOH was refined with restraints (DFIX, ISOR) and modelled as half occupied. Hydroxide hydrogen atoms on all MeOH (coordinated and uncoordinated) as well as ligand OH moieties were located and refined with restraints (DFIX). Two acetonitrile solvates were also modelled with restraints (ISOR). In **3**, all MeOH molecules were modelled as half occupied with restraints (DFIX, ISOR). One MeOH (C32–O33) is on the three fold axis and the hydrogens are modelled with an occupancy of 0.16667. Large voids are present in **3** of *ca.* 227 Å^3, with a total of 689 Å^3 per unit cell. SQUEEZE[43] was used to verify that the void volume does not contain any electron density.

Crystal data and details of data collection and refinement of compounds **2** and **3** are summarized in Table S1.† CCDC 1882361–1882362.†

Electrochemistry

Electrochemical measurements were carried out in DMF containing 0.1 M Bu_4NPF_6 in a classical three-electrode cell by cyclic voltammetry (CV) and rotating-disk voltammetry (RDV). The working electrode was a glassy carbon disk (GC, 3 mm in diameter), the auxiliary electrode a Pt wire, and the pseudo reference electrode a Pt wire. The cell was connected to an Autolab PGST, AT30 potentiostat (Eco Chemie, Holland) driven by a GPSE software running on a personal computer. All potentials are given *vs.* Fc^+/Fc used as internal reference and are uncorrected from ohmic drop.

Chemical oxidation

Optimization of oxidation of benzyl alcohol to benzaldehyde. All reactions were carried out in 1 mL glass vial under oxygen atmosphere, unless otherwise noted.

In a typical experiment: to a 1 mL glass vial containing a Teflon-coated magnetic stir bar was added cluster catalyst (2.3 mg, 0.60 μmol, 1.0 mol%), TEMPO (2.1 mg, 0.013 mmol, 22 mol%), benzyl alcohol (6.4 μL, 0.060 mmol, 1.0 equiv.), followed by the addition of DMF (300 μL). The contents of the vial were flushed with oxygen for *ca.* 2 minutes. The vial was then quickly sealed and the reaction mixture magnetically stirred for 24 h in sand bath that was maintained at an internal temperature of 140 °C using an electronic thermocouple. The reaction vial was then removed from the sand bath and allowed to cool to RT. 500 μL of ethyl acetate was added to the mixture, and the solution was centrifuged until separation of the solid catalyst was achieved. A sample for GC-MS analysis was prepared by removing 10 μL of the liquid phase from the reaction, followed by dilution with ethyl acetate (190 μL).

Results and discussion

Previously, we have demonstrated that depending on the reactants, the face-bridging ligands of the Mn_{19} system can either be N_3, Br, Cl, OMe or OH.[9–14] Herein, refluxing a mixture of $H_3\mathbf{L}^{\mathbf{Me}}$ and $MnBr_2{\cdot}4H_2O$ in the presence of Et_3N in MeCN/MeOH (5/1, v/v) afforded $[Mn^{III}_{12}Mn^{II}_7(\mu_4\text{-}O_8(\mu_3\text{-}OCH_3)_2(\mu_3\text{-}Br)_6(H\mathbf{L}^{\mathbf{Me}})_{12}(MeOH)_6]Br_2$ (**2**). When a similar reaction was carried out with $MnCl_2{\cdot}4H_2O$ as source of Mn and in the additional presence of $Sr(NO_3)_2$, the compound $[Mn^{III}_{12}Mn^{II}_6Sr(\mu_4\text{-}O_8(\mu_3\text{-}Cl)_8(H\mathbf{L}^{\mathbf{Me}})_{12}(MeCN)_6]Cl_2$ (**3**) was obtained. Single crystal X-ray analyses revealed that the compounds crystallize in the monoclinic $P2_1/n$ (**2**) and the trigonal $R\bar{3}$ (**3**) space groups, with two and three molecules, respectively in the unit cell. The results of the X-ray structural analysis are summarized in Table S1.† The crystal structure of **2** and **3** are given in Fig. 1.

The core of **2** and **3** are isostructural to the topology of the previously reported $\{Mn_{19}\}$ and $\{Mn_{18}M\}$ complexes[9–14] and can be considered as consisting of two supertetrahedral $\{Mn^{III}_6Mn^{II}_4\}$ units sharing a common Mn^{II} vertex (**2**) or two supertetrahedral $\{Mn^{III}_6Mn^{II}_3Sr\}$ units sharing a common Sr vertex (**3**). Compounds **2** and **3** slightly differ from the previously reported analogues. For instance, compound **2** differs

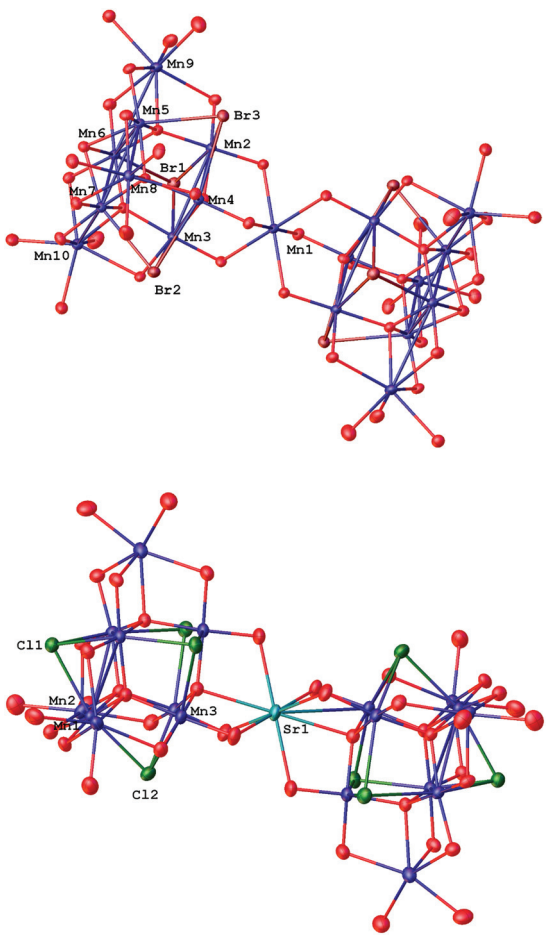

Fig. 1 Symmetry unique metal/halide labelled core only diagrams of **2** (upper) and **3** (lower). All solvents, hydrogen, carbon and nitrogen atoms omitted for clarity. A full diagram of each molecule is given in the ESI.† Atomic displacement shown at 50% probability.

from the original Mn_{19} aggregate (**1**),[9] as well as the analogous compound $[Mn^{III}_{12}Mn^{II}_{7}(\mu_4\text{-}O)_8(HL^{Me})_{12}(\mu_3\text{-}Br)_7(\mu_3\text{-}OH)(MeCN)_6]Br_2$ (**4**),[12] in terms of their μ_3-face-bridging ligands. In **2**, the two face-bridging ligands on the molecular threefold axis are both (μ_3-OMe) unlike in compound **1** and **4** where these are made up of μ_3-N_3 (**1**) or μ_3-Br and μ_3-OH (**4**) ligands, respectively. Compound **2** also differs from **4** in the composition of the six terminal ligands on the outer Mn^{II} vertices of the supertetrahedron. In **2**, these are MeOH while in **4** these are exclusively MeCN as in compound **1**. It should be pointed out here that while similar solvent mixtures (MeCN/MeOH, 5/1, vol/vol) were employed for these reactions, the reason for the observed differences in structural composition is unclear. Moreover, all attempts to completely substitute the face-bridging ligands with μ_3-Br by using excess bromide source were unsuccessful. We have also previously reported a Mn_{19} aggregate, $[Mn^{III}_{12}Mn^{II}_{7}(\mu_4\text{-}O)_8(HL^{Me})_{12}(\mu_3\text{-}Cl)_6(\mu_3\text{-}OMe)_2(MeOH)_5(MeCN)]Cl_2$ (**5**),[12] where the two face-bridging ligands on the molecular threefold axis are both μ_3-OMe as observed in **2**. In **5**, six of the face-bridging ligands are chlorides, hence compound **2** is a new analogue of the Mn_{19} system.

Electrochemistry

Investigations of the species were carried out by cyclic voltammetry and rotating disk voltammetry (RDV) in DMF +0.1 M Bu_4NPF_6. The electrochemical data for compound **2** and **3** are shown in Table 1.

In oxidation, cyclic voltammetry (CV) of **2** showed two successive irreversible peaks measured at −0.12 V and 0.42 V *vs.* Fc^+/Fc measured without Fc after the reduction of **Mn_{19}** (**2**) (Fig. 2, red curve with initial scanning direction to negative potential, explicitly reduction followed by the oxidation) while RDV presented only one wave at 0.33 V *vs.* Fc^+/Fc (Fig. S3,† left). It should be pointed out that, the first peak detected from CV at −0.12 V was not measured in the case of the initial scanning direction to positive potential (Fig. 2, black curve), namely oxidation followed by the reduction. The potential of the only irreversible peak observed was measured at 0.27 V (measured in the absence of Fc), a value close to the potential obtained from RDV (Fig. S3†). Thus, the first peak may be due to the re-oxidation of the reduced compound **2**, which might evolve after reduction to give a different oxidation potential for the Mn(III/II) redox couple. Alternatively, the first signal might be due to adsorption of the reduced compound **2** at the GC electrode, which renders the Mn atoms easier to oxidize. Because of such adsorption the coulometry is difficult to be done and give important variability of the value for the number of electron exchanged measured. The wave from CV at 0.27 V corresponds to the irreversible oxidation of the seven Mn(II) atoms to Mn(III) according the molecular structure of $[Mn^{III}_{12}\mathbf{Mn^{II}_{7}}(\mu_4\text{-}O_8(\mu_3\text{-}OCH_3)_2(\mu_3\text{-}Br)_6(HL^{Me})_{12}(MeOH)_6]Br_2$ (**2**). Controlled potential coulometry under continuous argon bubbling and stirring at applied potential of 0.4 V has been conducted several times and consumes between 6.8 to 7.4 electrons per molecule. Indeed, we have done two exhaustive oxidations giving 6.8, and 7.4 electrons exchanged. The fluctuation of the number of electron exchanged is probably due to the adsorption of compound (**2**) at the electrode which strongly alter the measurements.

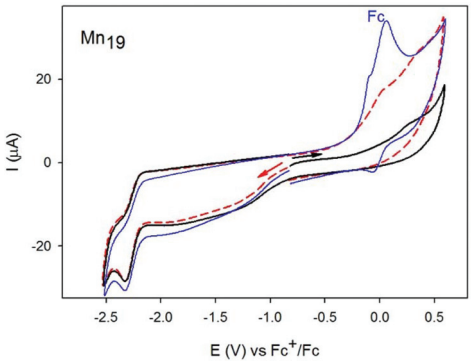

Fig. 2 Cyclic voltammetry of Mn_{19} (**2**) at a scan rate of 0.1 V s^{-1} in DMF 0.1 M $TBAPF_6$ with Fc (blue curve) and without Fc (black and red curves), c = 1 mM. The arrow as well as the color of the curves (black or red) indicate the beginning and sweep direction of the voltammetric scan. Black curve: initial scanning direction to negative potential [reduction of Mn_{19} (**2**)] followed by a reverse sweep back in order to join the oxidation wave. Red curve: initial scanning direction to positive potential [oxidation of Mn_{19} (**2**)].

Table 1 Electrochemical data for **2** and **3** in DMF (+0.1 M Bu_4NPF_6 against Fc^+/Fc)

	CV			RDV
Species	$E^{\circ a}$,V/Fc^+/Fc	$\Delta E_p{}^b$, mV	E_p,^{c} V/Fc^+/Fc	$E_{1/2}{}^d$, V/Fc^+/Fc
Mn_{19} (2)			0.42	0.33
			−1.29	*d*
			−1.89	*d*
	−2.25	90		
$Mn_{18}Sr$ (3)			0.25	0.29
			−1.20	−1.20
			−1.75	−1.75
			−2.10	−2.16

[a] $E^\circ = (E_{pc} + E_{pa})/2$, where E_{pc} and E_{pa} correspond to the cathodic and anodic peak potentials, respectively. [b] $\Delta E_p = E_{pa} - E_{pc}$. [c] E_p = irreversible peak potential. [d] Due to important adsorption at the electrode, the RDV in the cathodic domain is ill defined and is not exploitable.

For the **$Mn_{18}Sr$** cluster (**3**), in oxidation, cyclic voltammogramm (CV) showed only one irreversible peaks at 0.25 V *vs.* Fc^+/Fc. RDV presented also only one wave at 0.29 V *vs.* Fc^+/Fc (Fig. S4†). The first peak detected might be due to the oxidation of the six Mn(II) atoms to Mn(III). Such behaviour is similar to **2** compound except that the six Mn(II) are easier to be oxidized (0.25 V *versus* 0.43 V).

In the cathodic domain, CV showed three successive reductions. The first two reductions are irreversible and ill-defined at −1.29 V and −1.89 V, while the last reduction was reversible at −2.25 V (ΔE_p = 90 mV) *vs.* Fc^+/Fc peaks. Due to significant adsorption at the electrode, the RDV in the cathodic domain is ill-defined and is not exploitable (Fig. S3†). Thus

for compound **3**, the presence of the Sr atom does not affect strongly the redox behaviour in reduction. In oxidation, the oxidation of the Mn(II) are 180 mV easier to be oxidized than for **2**. The redox behaviour in reduction is also similar to **2** showing three successive steps but 90, 140 and 150 mV easier to be reduced than for **2**, respectively.

Catalytic oxidation

The ability of compounds **2** and **3** to act as catalysts for the partial chemical oxidation of benzyl alcohol to benzaldehyde was investigated. In analogy with previous catalytic oxidations using manganese clusters,[33] our initial investigations employed **2** (typically 1 mol%) with benzyl alcohol (1 equiv.) and TEMPO (22 mol%) in DMF under an oxygen atmosphere (1 atm). GC-MS analysis of reactions carried out in a variety of solvents after 18 h at 100 °C indeed confirmed that DMF was the most efficient, likely due to the high solubility of the catalyst in that solvent (see Table S2†).

After optimization of temperature and time, it was found that after 24 h at 140 °C, 74% conversion to benzaldehyde was achieved without observable accompanying over-oxidation to benzoic acid (Table 2, entry 1). Further optimisation and control experiments were carried out to better understand the reaction. Oxidation is observed in the absence of catalyst, but in roughly one third the yield (entry 2). Lower reaction temperatures were not suitable (entries 3–4). A catalyst loading of 1 mol% was found to be optimal, with higher or lower loadings leading to poorer yields (entries 5–7). Leaving out TEMPO does not completely stop the reaction but leads to lower yields (entry 8). In the presence of TEMPO, using air instead of O_2 or even conducting the reaction under an Ar atmosphere still does not completely inhibit the reaction (entries 9–10), showing that the ultimate source of oxidant is *flexible*. However, an oxidant is nonetheless required, since omitting TEMPO and using air instead of O_2 at the same time leads to a drastic drop in yield (entry 11).

Table 2 Influence of conditions on the chemical oxidation of benzyl alcohol catalysed by Mn_{19} **2**

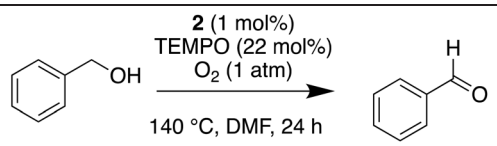

Entry	Deviation from standard conditions[a,b]	Alcohol (%)	Aldehyde (%)
1	None	26	74
2	No **2**	78	22
3	120 °C instead of 140 °C	70	30
4	100 °C instead of 140 °C	95	5
5[c]	5 mol% **2** instead of 1% mol%	80	20
6[c]	10 mol% **2** instead of 1 mol%	100	0
7[c]	0.1 mol% **2** instead of 1 mol%	79	21
8[c]	No TEMPO	48	52
9	Air instead of O_2	53	47
10	Ar instead of O_2	54	46
11[c]	No TEMPO and air instead of O_2	89	11

[a] Reaction conditions: Oxygen (1 atm), benzyl alcohol (0.06 mmol), TEMPO (22 mol%), Mn_{19} **2** (1 mol%) in 1 mL of DMF, at 140 °C; 48 h. [b] PhCHO was the only product; no $PhCO_2H$ acid was detected by GC-MS. [c] Reaction run for 48 h.

Table 3 Influence of various conditions in the chemical oxidation of benzyl alcohol by $Mn_{18}Sr$ **3**

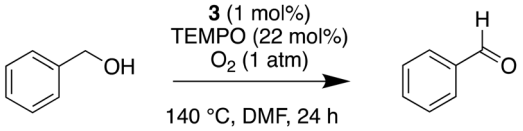

Entry	Deviation from standard conditions[a]	Alcohol (%)	Aldehyde[b] (%)
1	None	54	46
2	No TEMPO	35	65
3	Air instead of O_2	49	51
4	Ar instead of O_2	55	45
5	No TEMPO and air instead of O_2	65	35

[a] Reaction condition: Oxygen (1 atm), benzyl alcohol (0.06 mmol), TEMPO (22 mol%), $Mn_{18}Sr$ **3** (1 mol%) in 1 mL of DMF, at 140 °C; 24 h. [b] PhCHO was the only product; no $PhCO_2H$ acid was detected by GC-MS.

The oxidation of benzyl alcohol was also evaluated with $Mn_{18}Sr$ (**3**) under the same conditions (Table 3). The $Mn_{18}Sr$ catalyst gives slightly lower yields compared to Mn_{19} and over-oxidation is again not observed. One notable observation is that the $Mn_{18}Sr$ catalyst works best in the absence of TEMPO (entry 2), in departure from oxidation reactions catalysed by $CeMn_6$ clusters previously reported by Christou and co-workers.[33] In that prior report, the Ce atom was found to be the active component in the catalytic oxidation, and served to oxidize TEMPO, which in turn oxidizes the alcohol. The presence of TEMPO was thus found to be essential to catalytic oxidation. In the present work, the observation that the $Mn_{18}Sr$ catalyst **3** is optimal in the absence of TEMPO indicates a change in mechanism, such that the catalyst itself is capable of oxidizing the alcohol with catalytic turnover. As expected, the yield drastically decreases if TEMPO, O_2 or both are removed (entries 3–5).

To determine whether the catalysts employed in the present study are stable under the reaction conditions, the solid catalyst was analysed by IR spectroscopy. The IR spectra of **2** and **3** before and after the reaction show some discrepancy (Fig. S9,† new bands appearing at 1300–1600 cm^{-1}), suggesting that the catalyst might have undergone some modification under the catalytic conditions. This is expected as we previously observed that the system undergoes ligand exchange and/or scrambling under certain conditions.[12]

Conclusions

We have reported new analogues of the {Mn_{19}} and {$Mn_{18}Sr$} aggregates, compounds **2** and **3** and demonstrated their cata-

lytic activity in the selective oxidation of benzyl alcohol to benzaldehyde in up to 74 and 65% yields, respectively. These values are comparable to those obtained by Christou *et al.* for similar cluster compounds.[33] The attractiveness of the $\{Mn_{19}\}$ system is that it can be further tuned to access a variety of functionalized $Mn_{19}(R)$ aggregates, where the interplay of the electronic contribution of the substituent R can be investigated, where R = the substituent at the 4-positon of the $H_3\mathbf{L}^{\mathbf{R}}$ ligand system. Moreover $\{Mn_{18}M\}$ (where M is a heterometals), are readily accessible and could be suitable candidates to explore the influence of heterometals on the redox-potential of the system and hence catalysis, even in the absence of organic co-catalysts. Linking these species to form one-, two- and three-dimensional extended arrays and evaluation of these compounds towards photo-catalytic water splitting (oxygen evolution) is also envisaged.

Conflicts of interest

There are no conflicts to declare.

Acknowledgements

This project has received funding from the European Research Council (ERC) under the European Union's Horizon 2020 research and innovation programme (grants agreements no. 639170 and no. 647719), from ANR LabEx "Chemistry of Complex Systems", and from Science Foundation Ireland (13/IA/1896).

Notes and references

1 C. S. Mullins and V. L. Pecoraro, *Coord. Chem. Rev.*, 2008, **252**, 416.
2 F. Troiani and M. Affronte, *Chem. Soc. Rev.*, 2011, **40**, 3119.
3 G. Aromí, D. Aguila, P. Gamez, F. Luis and O. Roubeau, *Chem. Soc. Rev.*, 2012, **41**, 537.
4 L. Zhang, R. Clérac, C. I. Onet, M. Venkatesan, P. Heijboer and W. Schmitt, *Chem. – Eur. J.*, 2012, **18**, 13984.
5 L. Zhang, R. Clérac, P. Heijboer and W. Schmitt, *Angew. Chem., Int. Ed.*, 2012, **51**, 3007.
6 L. Zhang, B. Marzec, R. Clérac, Y. Chen, H. Zhang and W. Schmitt, *Chem. Commun.*, 2013, **49**, 66.
7 T. O. Chimamkpam, R. Clérac, D. Mitcov, B. Twamley, M. Venkatesan and W. Schmitt, *Dalton Trans.*, 2016, **45**, 1349.
8 L. Zhang, T. Chimamkpam, C. I. Onet, N. Zhu, R. Clérac and W. Schmitt, *Dalton Trans.*, 2016, **45**, 17705.
9 A. M. Ako, I. J. Hewitt, V. Mereacre, R. Clérac, W. Wernsdorfer, C. E. Anson and A. K. Powell, *Angew. Chem., Int. Ed.*, 2006, **45**, 4926.
10 A. M. Ako, M. S. Alam, S. Mameri, Y. Lan, M. Hibert, M. Stocker, P. Müller, C. E. Anson and A. K. Powell, *Eur. J. Inorg. Chem.*, 2012, **26**, 4131.
11 S. Mameri, A. M. Ako, F. Yesil, M. Hibert, Y. Lan, C. E. Anson and A. K. Powell, *Eur. J. Inorg. Chem.*, 2014, **26**, 4326.
12 A. M. Ako, Y. Lan, O. Hampe, E. Cremades, E. Ruiz, C. E. Anson and A. K. Powell, *Chem. Commun.*, 2014, **50**, 5847.
13 A. M. Ako, V. Mereacre, R. Clérac, I. J. Hewitt, W. Wernsdorfer, C. E. Anson and A. K. Powell, *Chem. Commun.*, 2009, 544.
14 A. M. Ako, B. Burger, Y. Lan, V. Mereacre, R. Clérac, G. Buth, S. Gómez-Coca, E. Ruiz, C. E. Anson and A. K. Powell, *Inorg. Chem.*, 2013, **52**, 5764.
15 L. Bogani and W. Wernsdorfer, *Nat. Mater.*, 2008, **7**, 179.
16 W. Zhou, X. Zhao, Y. Wang and J. Zhang, *Appl. Catal., A*, 2004, **260**, 19.
17 B. Noheda, *Curr. Opin. Solid State Mater. Sci.*, 2002, **6**, 27.
18 S. Yonezawa and Y. Maeno, *Phys. Rev. B*, 2005, **72**, 180504(R).
19 T. G. Carrell, S. Cohen and G. C. Dismukes, *J. Mol. Catal. A: Chem.*, 2002, **187**, 3.
20 R. Tagore, R. H. Crabtree and G. W. Brudvig, *Inorg. Chem.*, 2008, **47**, 1815.
21 M. M. Najafpour, T. Ehrenberg, M. Wiechen and P. Kurz, *Angew. Chem., Int. Ed.*, 2010, **49**, 2233.
22 Z. Shi, C. Zhang, C. Tanga and N. Jiao, *Chem. Soc. Rev.*, 2012, **41**, 3381.
23 G. Zhan, Y. Hong, V. T. Mbah, J. Huang, A.-R. Ibrahim, M. Du and Q. Li, *Appl. Catal., A*, 2012, **439**, 179.
24 B. Wang, M. Lin, T. P. Ang, J. Chang, Y. Yang and A. Borgna, *Catal. Commun.*, 2012, **25**, 96.
25 J. Zhu, J. L. Figueiredo and J. L. Faria, *Catal. Commun.*, 2008, **9**, 2395.
26 C. Zhou, Z. Guo, Y. Dai, X. Jia, H. Yu and Y. Yang, *Appl. Catal., B*, 2016, **181**, 118.
27 C. Y. Ma, J. Cheng, H. L. Wang, Q. Hu, H. Tian, C. He and Z. P. Hao, *Catal. Today*, 2010, **158**, 246.
28 Q. Tang, X. Gong, P. Zhao, Y. Chen and Y. Yang, *Appl. Catal., A*, 2010, **389**, 101.
29 M. Yang, Q. Ling, R. Rao, H. Yang, Q. Zhang, H. Liu and A. Zhang, *J. Mol. Catal. A: Chem.*, 2013, **380**, 61.
30 M. Ilyas and M. Saeed, *Int. J. Chem. React. Eng.*, 2010, **8**, A77.
31 J. Zhu, K. Kailasam, A. Fischer and A. Thomas, *ACS Catal.*, 2011, **1**, 342.
32 L. Yao, L. Zhang, Y. Liu, L. Tian, J. Xu, T. Liu, D. Liud and C. Wang, *CrystEngComm*, 2016, **18**, 8887.
33 G. Maayan and G. Christou, *Inorg. Chem.*, 2011, **50**, 7015.
34 D. Sengupta, R. Bhattacharjee, R. Pramanick, S. P. Rath, N. S. Chowdhury, A. Datta and S. Goswami, *Inorg. Chem.*, 2016, **55**, 9602.
35 A. S. Borovik, *Chem. Soc. Rev.*, 2011, **40**, 1870.
36 G. Yin, *Coord. Chem. Rev.*, 2010, **254**, 1826.
37 K. P. Bryliakov and E. P. Talsi, *Coord. Chem. Rev.*, 2014, **276**, 73.

38 *APEX-3 v. 2016.9-0*, Bruker-AXS Inc., Madison, WI, 2016.
39 *SADABS v. 2016/2*, Bruker-AXS Inc., Madison, WI, 2016.
40 O. V. Dolomanov, L. J. Bourhis, R. J. Gildea, J. A. K. Howard and H. J. Puschmann, *Appl. Crystallogr.*, 2009, **42**, 339.
41 G. M. Sheldrick, *Acta Crystallogr., Sect. A: Found. Adv.*, 2015, **71**, 3.
42 G. M. Sheldrick, *Acta Crystallogr., Sect. B: Struct. Sci.*, 2008, **64**, 112.
43 A. L. Spek, *J. Appl. Crystallogr.*, 2003, **36**, 7.